



Synthesis, Structural, Optical, Physical and AC Conductivity Studies of Mg doped Nickel Nano Ferrites for multiple Applications

¹D. Mallesh and ^{1,2}Aravind Seema*

¹Department of Chemistry, Osmania University, Hyderabad-500007, India

²Department of Chemistry, University College of Science, Saifabad, Osmania University, Hyderabad-500007, India

Abstract: Nickel ferrite of chemical compositions $\text{Ni}_{1-x}\text{Mg}_x\text{Fe}_2\text{O}_4$ (where $x=0.0, 0.25, 0.5, 0.75$ and 1.0 with 0.25 variation) nanocrystalline materials were prepared using citrate-gel auto combustion route. The prepared sample's crystalline size and phase was confirmed by XRD, and the crystalline size was determined to be 26 to 28 nm using the Debye-Scherrer equation. The variations in lattice parameter of the samples indicates that it obeys Vegard's law. X-ray density of the sample found to be 6.58 to 5.10 gcm $^{-3}$. The SEM pictures show aggregated objects and particles that are in the nanometer range. According to stoichiometric ratio, elements are present (nickel, magnesium, iron, and oxygen) which confirmed by elemental dispersive spectroscopy (EDS). There are two FT-IR bands found in the FT-IR spectrum, that correspond to the stretching frequencies of the octahedral (ν_2) and tetrahedral (ν_1) bands. The optical absorption spectra revealed the decrease of cut-off wavelength and increasing trend of band gap energies. AC conductivity measurements revealed the increment of conductivity with an applied frequency and the Cole-Cole plots were resulted in the decrease of bulk resistance.

Keywords- Citrate gel auto combustion, Ni-Mg nano ferrites, XRD, SEM, FT-IR., Optical band gap, AC conductivity.

I. INTRODUCTION

Researchers have been attracted with magnetic nanoparticles for the past 20 years due to their adaptive and unique properties at extremely small dimension scale [1-3]. These materials may be employed in a variety of technological applications, including as sensors, biomedicine, the automotive industry, cooling systems, data storage, and converters. They also exhibit good magnetization, resistivity, and permeability [4]. Magnesium ferrite nanoparticles are among these magnetic materials as basically ferrites employed in a variety of applications because of their compositional and mechanical stability, great magneto crystalline anisotropy, Curie temperature, and high electrical resistivity [5, 6].

Due to their unique characteristics, the processes of synthesis, production, sintering, and control over the form and size of the particles may be adjusted. The sub lattices of tetrahedral (A-site) and octahedral (B-site) crystals, which make up the standard formula for spinel ferrites, are AB_2O_4 and AB_2O_3 , respectively. 16 trivalent and 8 divalent metal ions are combined to form the spinel unit cell, which is tightly packed in a FCC shape [7, 8]. The magnetic, electric, and optical properties are determined by the ratio of cation occupancy in A and B sites. Zinc and Fe^{3+} choose site B in Co ferrite, but most Fe^{3+} seek to conquer position A. Ferrites are ferrimagnetic substances with low dielectric loss and strong dielectric permittivity at various temperatures. These ferrite materials are also utilized in electric communications applications [9]. Grain size and grain boundaries are key factors in electrical characteristics, particularly in nanoferrite materials.

Spinel ferrites (MgFe_2O_4) are showing special interest and play a significant involvement in various applications due to its higher values of density, sensor application, photo-electrical properties. These materials can be used in the circulators, phase-shifting elements and also isolating elements. The optical properties of the MgO doped nickel ferrites are found good results. Nickel ferrite nano particles doped with MgO show excellent adsorption, opto-electrical related applications and also good bioactivity. In the current investigation, the MgO acting like a dopant and also nickel varying with respect to the dopant. The addition of MgO influences the original sites and the dopant occupies the site of host. The optical, structural and conductivity results are dependent on the modifier. The optical spectral analysis deals with different transitions in a materials.

Materials with smaller grains will have more pronounced grain boundaries. As a result, electron hopping between ions won't occur, boosting the resistivity and lowering material loss. Nickel ferrites and nickel ferrites doped with rare earths are of special interest to synthesis researchers due to their low cost and high curie temperature [10]. The present study, explores the synthesis of nickel magnesium ferrites $\text{Ni}_{1-x}\text{Mg}_x\text{Fe}_2\text{O}_4$ nano ferrites and to study the effect of dopant MgO on the structural, physical & optical properties, morphology and AC conductivity studies for suitability of the present NFs for multiple applications.

II. Experimental studies

Synthesis

The technique used was the citrate auto combustion method using a succession of $\text{Ni}_{1-x}\text{Mg}_x\text{Fe}_2\text{O}_4$ (where $x=0.0, 0.25, 0.5, 0.75$ and 1.0 with 0.25 variation) nano ferrites. Metal nitrates including Ni nitrate, magnesium nitrate, and ferric nitrate were each separately dissolved in deionized water in stoichiometric amounts. Citric acid was utilised as a chelating agent in a 1:3 ratio, followed by the formation of a homogenous solution, the dropwise addition of ammonia solution to the homogenous solution to preserve PH-7 neutrality, and through stirring of the solution on a magnetic stirrer. After being heated to a temperature of around 80°C , the whole solution was reduced to one-fourth of its initial volume. Temperature was then increased from 80°C to 150°C heated for an hour, causing a viscous gel to develop. The resultant ignited powder was then self-ignited and pounded in an agate mortar and pestle for at least 20 minutes. Residual substance from the furnace was crushed again in an agate mortar and pestle for one hour before being calcined for four hours at 500°C [11]. The powder was then analysed for structural conformation. The synthetic process stated in Fig.1 flow chart.

PREPARATION OF NANOPARTICLES PROCESS

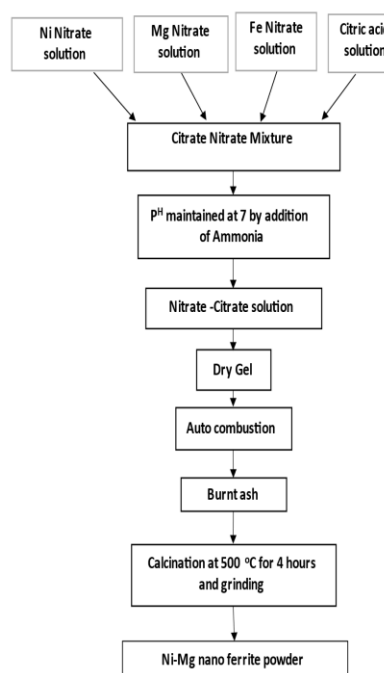


Fig.1. Flow chart for the preparation of nano particles

Characterization

The density was estimated through Archimedes method with Xylene as an immersion solvent. The optical spectra were recorded at room temperature in the wavelength range 200-1000nm with a resolution of 2nm. The frequency-based AC conductivity was analyzed using Jonscher power law and it was measured as a function of applied frequency and also with increasing temperature.

III. Results and Discussions

3.1 XRD studies of Ni-Mg nano-ferrites

The most common method for identifying a material's crystalline nature is X-ray diffraction examination. The crystalline structure of formed nanomaterials may be examined via a powder x-ray diffraction examination. Fig 2.indicates the X-ray diffraction pattern of $\text{Ni}_{1-x}\text{Mg}_x\text{Fe}_2\text{O}_4$ (where $x=0.0, 0.25, 0.5, 0.75$ and 1.0 with 0.25 variation) spinel nano ferrites. According to Fig.2 the powder X-ray diffraction (PXRD) pattern of Mg doped Ni Nano ferrites shows that the materials have a spinel structure and are crystalline, free of other impurity peaks [12].

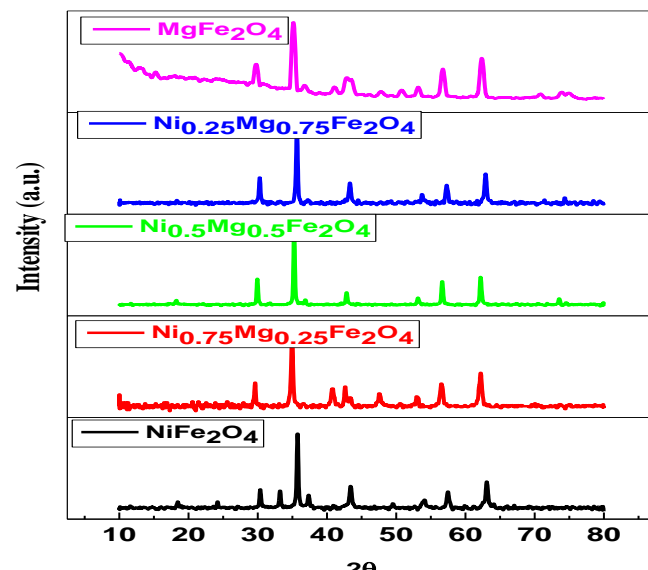


Fig.2. XRD pattern of $\text{Ni}_{1-x}\text{Mg}_x\text{Fe}_2\text{O}_4$ (where $x=0.0, 0.25, 0.5, 0.75$ and 1.0) spinel nano ferrites

An additional peak at 380 and 430 may be seen in the XRD pattern of Ni-Mg micro ferrites. The Ni-Mg Nano ferrite's XRD pattern exhibits Bragg reflection, a sign of its crystalline structure. The crystalline size, lattice constant, unit cell volume, and x-ray density of the samples were examined through x-ray diffraction examination. The Debye Schemer formula was used to determine the average crystalline size (l) of $\text{Ni}_{1-x}\text{Mg}_x\text{Fe}_2\text{O}_4$ (where $x=0.0, 0.25, 0.5, 0.75$ and 1.0 with 0.25 variation) nano ferrites samples [13].

Where λ = Wave length

β = Full width half maxima

Θ = Braggs angle

On magnesium ferrite, the crystalline size was found to vary between 26 and 28 nm, and it was increased as increasing dopant content of Mg. The ionic radius of Mg is the cause of the samples' varied crystalline sizes. The following formula gives the lattice parameter for the synthesized $\text{Ni}_{1-x}\text{Mg}_x\text{Fe}_2\text{O}_4$ (where $x=0.0, 0.25, 0.5, 0.75$ and 1.0 with 0.25 variation) nano ferrites.

Where h, k, l are miller indices.

As the doping Mg content on the Ni Nano ferrite lattice parameter was increased, the lattice parameter of the ferrite sample was observed to rise from 7.79 to 7.83 Å. It might be because Mg's ionic radius.

Volume of unit cell of the samples obtained from the following given formula.

Where a is a sample lattice parameter, the volume of unit cell changes from 473 to 480. All the materials x-ray densities are calculated by the following formula.

Where $Z =$ No. of molecules per unit cell. For the samples it is 8.

$M \equiv$ Molecular weight of samples.

M= Molecular weight
a= Lattice parameter

Pure NiFe₂O₄ sample x-ray density found to be 6.57 gm/cm³, whereas MgFe₂O₄ found to be 5.10 gm/cm³. The molecular weight and lattice parameter of the samples affect the X-ray density, which decreases with increasing Mg concentration. Pure Ni ferrite sample has the maximum X-ray density. Table.1 contains the tabulated values for all the above-mentioned parameters.

3.2 SEM Analysis of Ni-Mg nanoferrites

A high-resolution type of microscope called a SEM provides detailed analyses of materials. A scanning electron microscope may reveal the surface grains and grain boundaries of synthesized nanomaterials. SEM is a sophisticated method for understanding the topography, crystallography, and morphology of nanomaterials. The FE-SEM images of Ni-Mg nano ferrites are shown in Fig.3(a-c). All of the samples have agglomerated structures with irregularly distributed grain and grain boundary distributions. The resulting agglomerated structures show that the particle distribution in the samples is not uniform [14, 15].

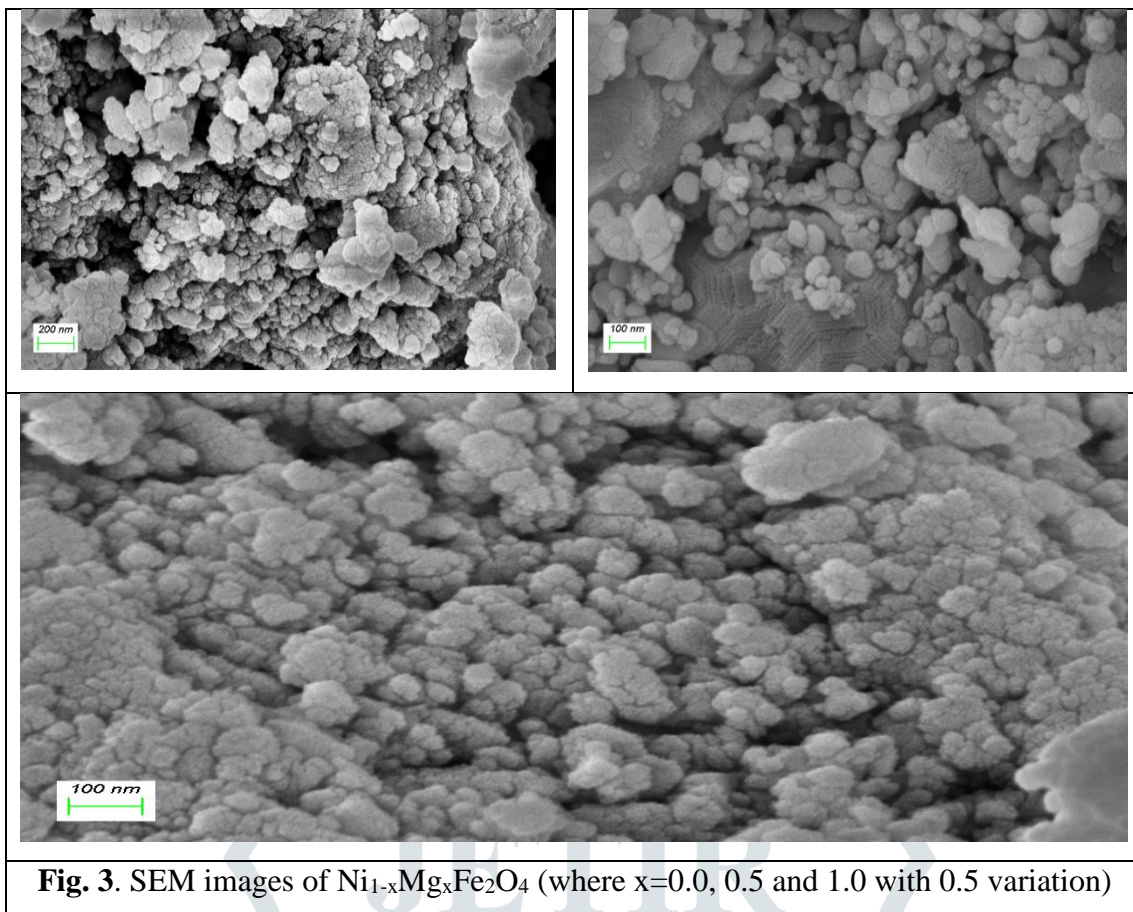
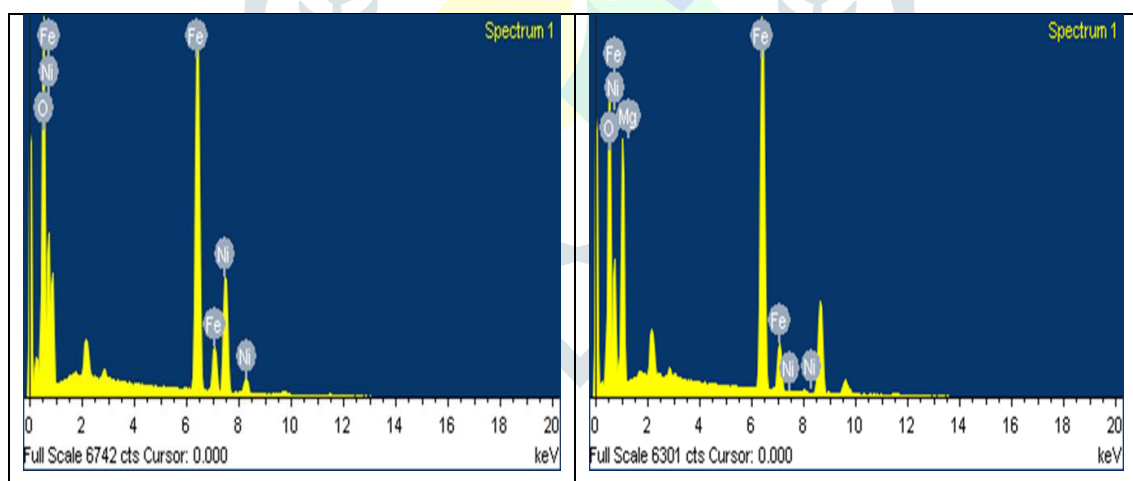
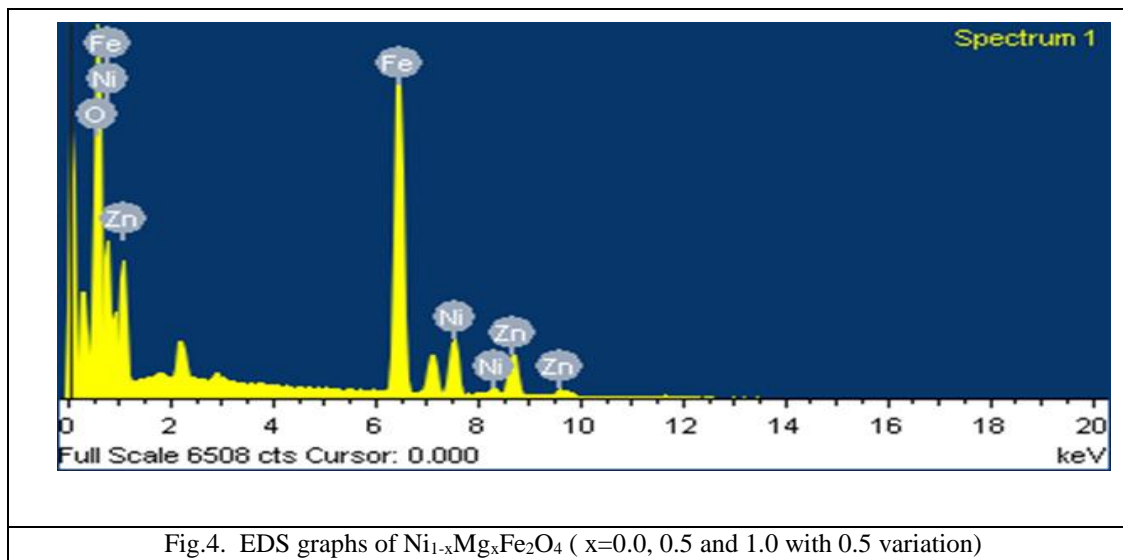


Fig. 3. SEM images of $\text{Ni}_{1-x}\text{Mg}_x\text{Fe}_2\text{O}_4$ (where $x=0.0, 0.5$ and 1.0 with 0.5 variation)

3.3.EDS spectral analysis of Ni-Mg nanoferrites

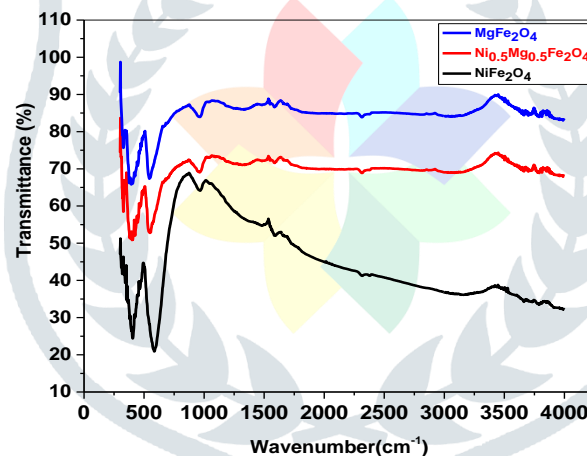
EDS is a method of analysis used to ascertain the chemical composition of the samples as well as their elemental analysis. The EDS spectrum graphs of Mg doped Ni nano ferrites are shown in Fig.4 (a-c). We can see from these spectral graphs that there are just the elements Ni, Mg, Fe, and O present. According to stoichiometric ratio, these graphs also show the samples' atomic and elemental percentages. Table.2 displays the atomic and elemental composition percentages that were provided.



Fig.4. EDS graphs of $\text{Ni}_{1-x}\text{Mg}_x\text{Fe}_2\text{O}_4$ ($x=0.0, 0.5$ and 1.0 with 0.5 variation)

3.4 FT-IR STUDIES of Ni-Mg nanoferrites

The functional group of the synthesized substance may frequently be determined from FTIR spectra. The alignment of chemical bands, the cation distribution, and the creation of the spinal structure may all be examined using this spectroscopy. Metal cations are deposited in the tetrahedral and octahedral sublattices of two sub-lattices of the ferrite structure. An FTIR spectrophotometer with a range of 200–4000 cm^{-1} KBr was used as a reference at room temperature [16, 17]. The FTIR spectra of $\text{Ni}_{1-x}\text{Mg}_x\text{Fe}_2\text{O}_4$ (where $x=0.0, 0.5$ and 1.0) nanoferrites are shown in Fig.5. Two broad peaks in the higher wave number area of 600 cm^{-1} and the lower wave number region of 400 cm^{-1} were visible in these spectral graphs. The 400 cm^{-1} peak corresponds to the M-O band of the octahedral site (B-site), while the 600 cm^{-1} peak is related to the stretching frequency of the tetrahedral site (A-site). While the doping Mg content in Ni ferrite peak position may vary due to the variation of Mg^{2+} concentration and ionic radius.

Fig.5. FT-IR spectrum of Mg-Ni nano-ferrites $\text{Ni}_{1-x}\text{Mg}_x\text{Fe}_2\text{O}_4$ (where $x=0.0, 0.5$ and 1.0 with 0.5 variation)

3.5 Optical parameters of Mg doped Nickel ferrites

The density of the Mg-doped nickel ferrites was increased with increment of dopant MgO in a linear way. Initial density was found as 4.93 g/cm^3 . With increasing MgO , it was increased upto 5.36 g/cm^3 as shown in Fig.6. In the Fig.7, the absorption spectra of Mg-doped nickel nano ferrites was shown graphically. It is very clear that the cut-off wavelength of the spectra is decreasing with the additive MgO content linearly. It varied in between 492nm to 469nm . The initial cut-off value of the pure sample is the highest and dopant concentration results in the decrease of cut-off. The lowest cut-off value found for the high MgO dopant concentration. The bridging oxygens will be enhance in the sample so that less randomness can be seen. It is reflected in the results of Urbach energy [18]. The evaluated optical parameters were shown in the Table.3.

The indirect band gap (E_{ind}) values of the MgO dopant nickel NFs were calculated with extrapolation the linear region of the graph towards X-axis to meet at $(\alpha h\nu)^{1/2} = 0$ as a function of incident photon energy. Fig.8. represents the Tauc's plots for evaluating indirect bandgap energy. It was increased with the addition of the dopant MgO . The right shift of bandgap indicates the creation of bridging oxygens BOs and improvement of the properties. Sample containing high MgO exhibits highest band gap energy.

The direct band gap (E_{ind}) values of the MgO dopant nickel NFs were calculated with the graph drawn $(\alpha h\nu)^2 = 0$ as a function of incident photon energy. Fig.9 represents the Tauc's plots for evaluating direct bandgap energy. It was increased with the addition of the dopant MgO . The right shift of bandgap indicates the creation of bridging oxygens BOs and improvement of the properties. Sample containing high MgO exhibits highest band gap energy.

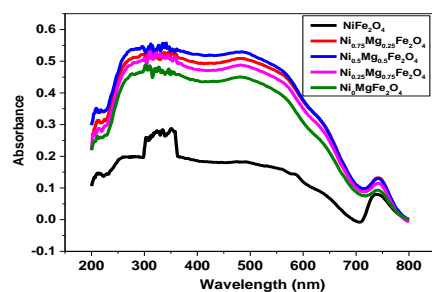


Fig.7. Optical absorption spectra of MgO doped Nickel ferrites

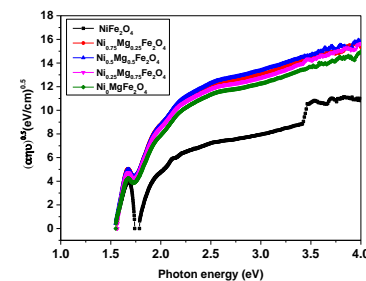


Fig.8. Optical absorption spectra of MgO doped Nickel ferrites

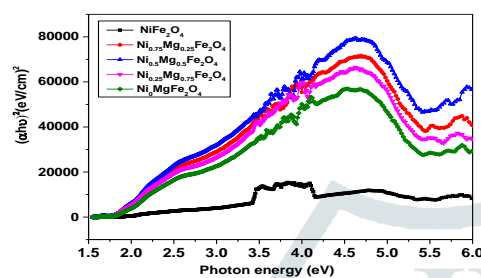


Fig.9 Direct band gap of MgO doped Nickel ferrites

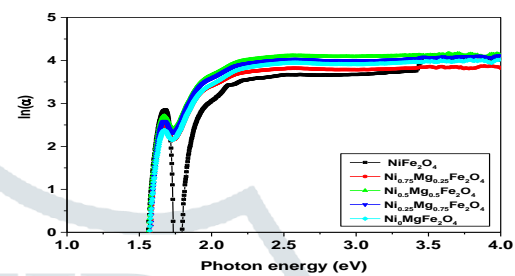


Fig.10 Urbach plots of MgO doped Nickel ferrites

The Urbach energy of the present MgO dopant NFs was found to decrease with increase in the Mg-dopant content as shown in the Fig.10. It is an indication that enrichment of rare-earth oxide into ferrite base results in more order and decrease of disorderness [19]. It is because of bridging oxygens generated in the ferrite sample. The refractive index also enhanced with adding the MgO from 1.18 to 1.38.

3.6. AC conductivity of Magnesium doped nickel ferrites series

MgO doped nickel nano ferrites Ni Fe₂O₄

Fig.11 shows the variation in AC conductivity with frequency and temperatures of Mg doped Nickel nano ferrites Ni0.75Mg0.25Fe2O4 for 0.20 mole percent of dopant. It found that the of Magnesium doped nano ferrites NFs has shown the dispersive character at the lower temperatures like RT etc. The impurities present in the synthesized ferrites are the reasons for the dispersion behaviour. of Ni0.75Mg0.25Fe2O4 sample found to vary only one order in the low applied frequency domain , whereas, at high frequencies it also varied upto two orders. The conductivity is enhanced up to two orders when the temperatures raised.

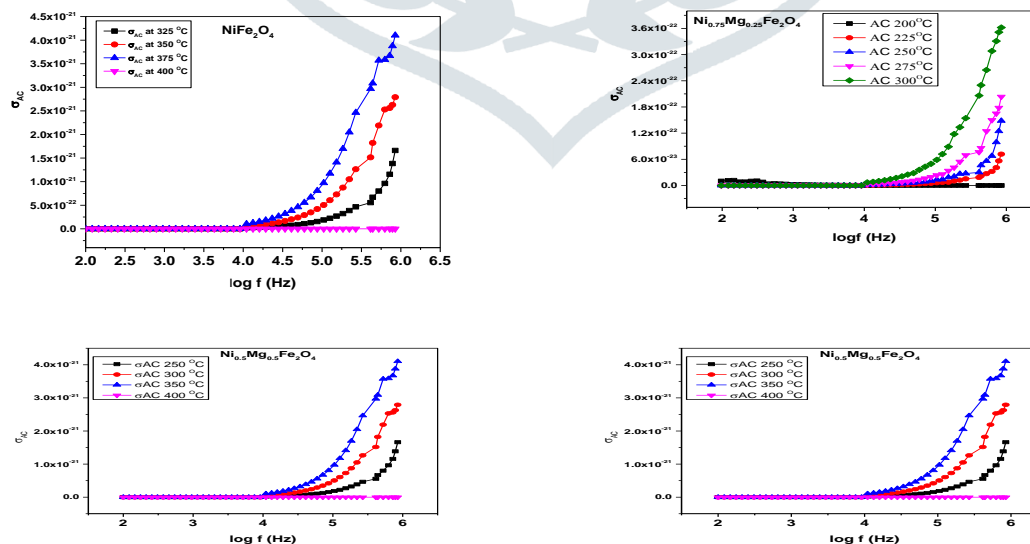


Fig.11. AC conductivity variation with frequency of Magnesium doped nickel ferrites

Z/ vs Z// Cole-Cole plots:

Dielectric dispersion behaviour of the synthesized magnesium MgO doped NiMgFe₂O₄ nickel nano ferrites have been studied from RT to 450oC. Good results obtained at high temperatures like 200oC, 250oC, 300oC, 350oC, 400oC and 450oC for all the studied nano ferrites dope with Mg. Dielectric behaviour with impedance data have been discussed with real Z/ and imaginary complex components Z//. The Plots of real and imaginary parts were given a single semicircle at the high and lower temperature. It might be attributed to the small polarons hopping mechanism and also bulk resistance. Cole-Cole impedance plots of the pure and Mg dope nickel nano ferrites have shown semicircles [20-22].

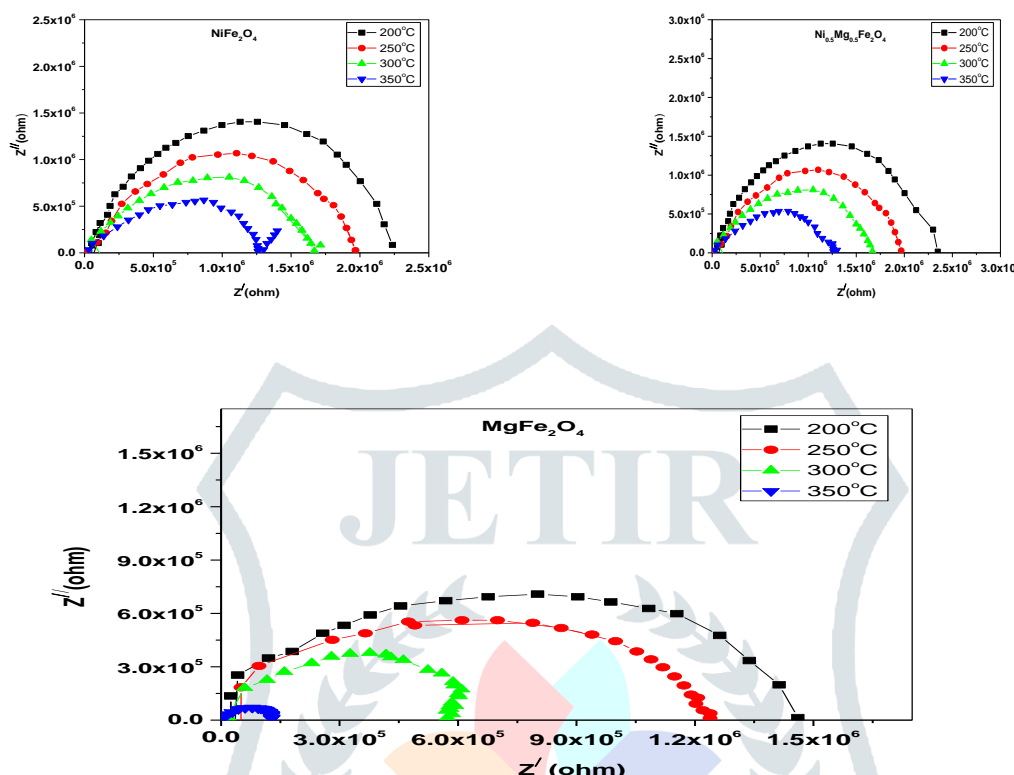


Fig.12. Cole-Cole impedance plots of Magnesium doped nickel ferrites

Cole-Cole impedance plots of MgO dope nickel nano ferrites were shown in the Fig.12 and was observed the semi-circular behaviour for different temperatures. The bulk resistance (R_b) of the semi-circular impedance plots of the ferrites samples was decreasing with increase of temperature, also with Mg content. The inner radius of the semicircle arcs was decreased with increasing the temperature and also with dopant content [23-26]. The bulk resistance found to the lowest for highest content of dopant Mg. The bulk resistance play a key role in the plots and the plots almost equivalent to the R-C network of the electric circuit. Good results were found for higher values of the temperatures like 300oC, 350oC, 400oC and 450oC.

Dielectric constant of Ni-Mg series

Dielectric constant relates the relation between the capacitance in medium (C) and to the vacuum (C₀). Fig.13 shows the variations of dielectric constant (ϵ') real portion of MgO doped nickel nano-ferrites. It is understood from the figure is that the real part of dielectric constant decreased with increasing the applied frequency [27-28]. It found the highest in the lower frequency region and suddenly decreased with increasing the frequency which may be due to changes of relaxation mechanism in the nano ferrite samples. It was almost saturated in the high frequency region.

The variation of dielectric constant real part of Mg dope nickel nano ferrites with applied frequency were shown in the Fig.13. Generally, a material composed of high conducting grains and less conducting grain boundaries. Especially, ferrites obeys that the dielectric constant is proportional to square root of conductivity. Therefore, it is high at lower frequencies and then decrease with increase of frequency. Dielectric constant also depends on the mobility of electronic charge carriers. Finally, one can understand that the dielectric constant decrease with frequency. It may also attributed to the electron exchanging mechanism in the Oh octahedral sites Fe²⁺ and Fe³⁺ ions.

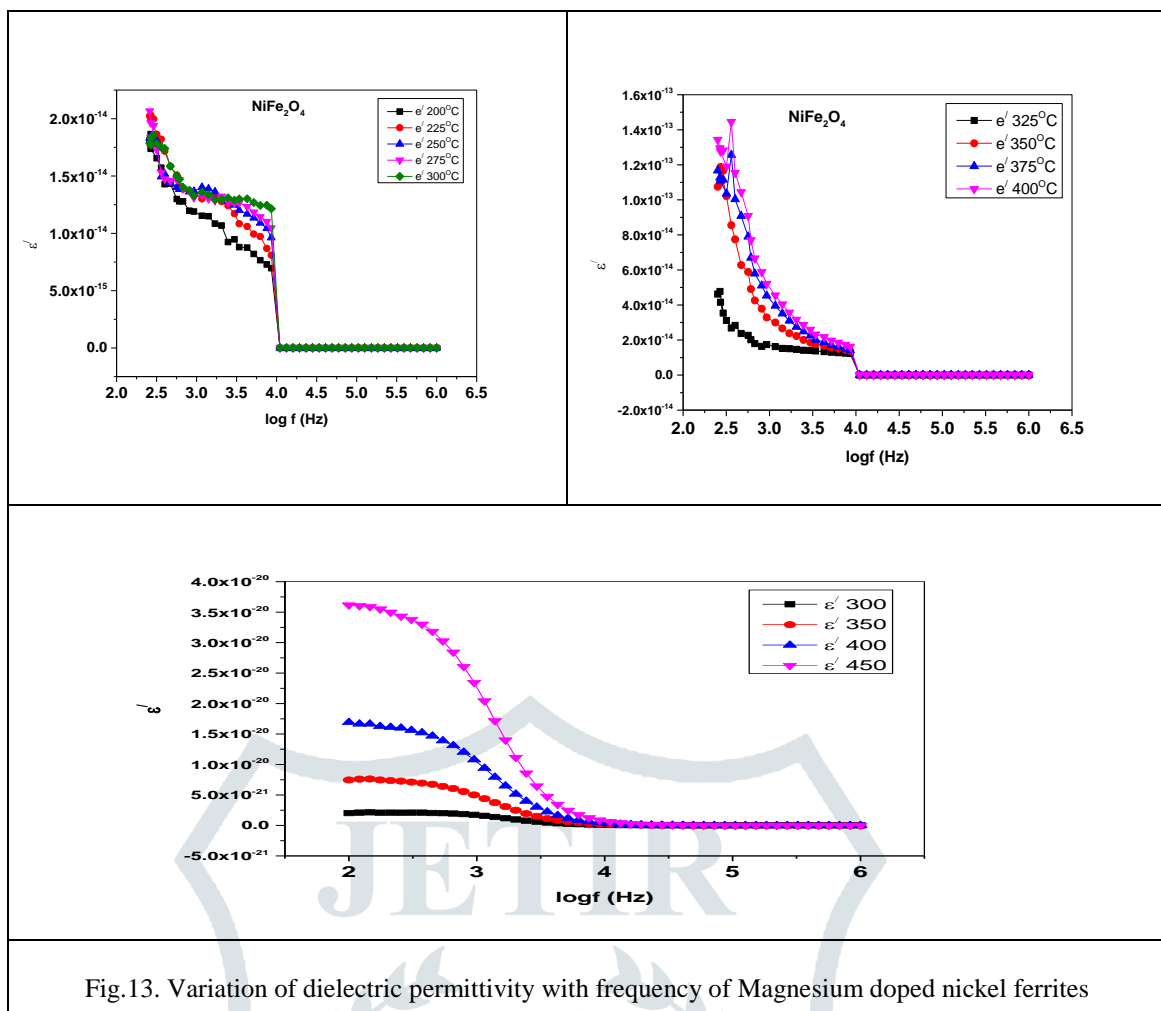


Fig.13. Variation of dielectric permittivity with frequency of Magnesium doped nickel ferrites

Tan δ of Ni-Mg series

Dielectric loss closely associated with energy dissipation in dielectric materials. Fig.14 depicts the variation of $\tan\delta$ with logarithm of frequency at different temperatures of synthesized MgO doped nickel nano ferrites. Dielectric loss tangent values are high at lower frequencies for all the prepared samples. The dielectric loss tangent values decreased with frequency increment.

The present studied NFs obeys Koop's model theory which states the decrease of tangent loss with applied frequencies. The dielectric loss tangent ($\tan\delta$) explains the dissipation of energy of materials especially in dielectric materials. The variation of $\tan\delta$ with applied frequency ($\log f$) of Mg doped nickel ferrites have shown in the Fig.14. At various temperatures the variation of loss tangent was studied. It found to be decrease with increasing frequency upto certain value and gets saturated at the higher frequencies. The decrease of loss tangent may be due to the increment of charge carriers and decrease in the relaxation time [29-31].

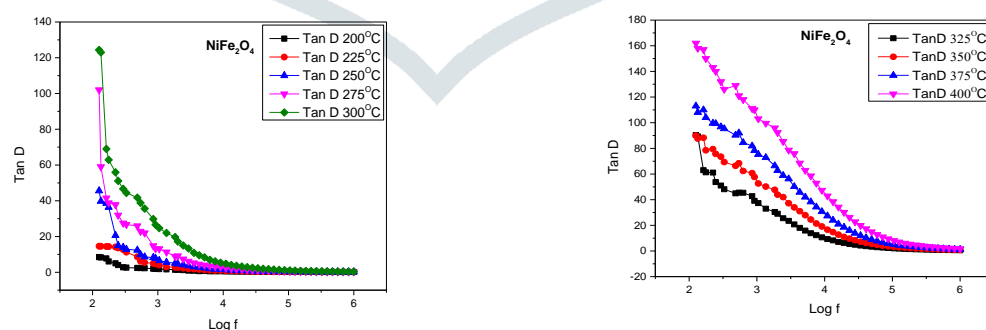


Fig.14. Variation of dielectric loss with frequency of Magnesium doped nickel ferrites

In this study, the decrement of dielectric loss tangent with respect to the frequency clears that synthesized nano ferrites are in the dielectric character. Dielectric loss tangent decreases with temperature due to mobility of charge carrier increases and decrease in relaxation time. Relaxation time is inversely proportional to the dielectric loss. All the synthesized NF samples showed the similar trend for the pure, Mg dope and NiO containing nickel NF samples [32-33].

At a specific temperature, all the electrical conductivity plots (log₁₀ changes in slope due to the Curie temperature were shown in the Fig.15. The temperature at which a ferri-magnetic material changes to a paramagnetic state [34-36]. The curie temperature discontinuity is due to the magnetic transition from a ferromagnetic state to a paramagnetic state. The electrical resistivity and thermal activation energies of the prepared samples in the ferri-magnetic and paramagnetic regions confirmed their nano characteristics [37-39]. The discontinuity of the Arrhenius plots is due to the conduction mechanism changing [40-43]. The synthesised sample has a favourable conduction mechanism because of the exchange of electrons between Fe²⁺ and Fe³⁺ ions in octahedral sites.

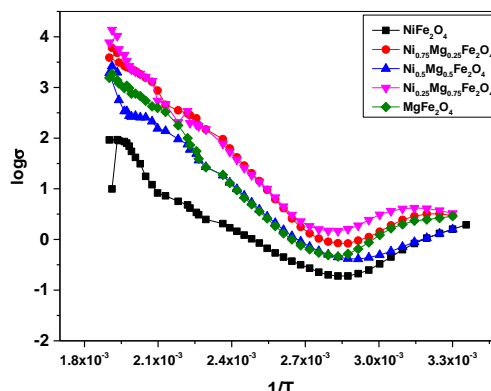


Fig.15. DC conductivity (Arrhenius plots) of Mg doped nickel ferrites

IV. Conclusions

- Though citrate gel auto combustion method a series of Ni_{1-x}Mg_xFe₂O₄ (where x=0.0, 0.25, 0.5, 0.75 and 1.0 with 0.25 variation) spinel nano ferrites successfully prepared at low temperature.
- Single phase cubic spinel structure of the synthesized samples conformed by x-ray diffraction analysis.
- Lattice parameter of the sample increased with increasing the dopant content of magnesium.
- Volume of unit cell variation also observed with substitution of Mg.
- The cut-off wavelength is varied between 492nm to 469nm. The initial cut-off value of the pure sample is the highest and dopant concentration results in the decrease of cut-off. The highest indirect band gap recorded for pure sample.
- Two broad band appeared in FT-IR spectrum, which attributes the tetrahedral and octahedral sites conforms the spinel structure.
- The AC conductivity was increased with an increase of log₁₀ and also with increasing temperature.
- The dielectric loss tangent decreased with increasing frequency
- The dielectric constant real part decreased with increasing frequency
- The Cole-Cole plots were showed the semi-circular trend with decreasing radius
- The bulk resistance decreased with increment of temperature. The present nano ferrites are the suitable candidates for optoelectronic device applications and also for magnetic recording chip applications.

V. ACKNOWLEDGMENT

The authors are thankful to the Head, Department of Chemistry, Osmania University, Hyderabad-500007 for providing the FT-IR, Optical study facilities. The authors also thankful to Head, Department of Physics, Osmania University for the Density and XRD facility.

REFERENCES

- [1] Ali, A. 2001. Macroeconomic variables [1]. P. Anantha Rao, V. Raghavendra, B. Suryanarayana, T. Paulos, N. Murali, P.V.S.K. Phanidhar Varma, R. Giri Prasad, Y. Ramakrishna, K. Chandramouli, Cadmium substitution effect on structural, electrical and magnetic properties of Ni-Zn nano ferrites, Results Phys. 19 (2020) 103487. <https://doi.org/10.1016/J.RINP.2020.103487>.
- [2]. M. Veena, G.J. Shankaramurthy, H.S. Jayanna, H.M. Somashekharappa, Effect of γ - rays irradiation on structural, electrical and magnetic properties of Dy³⁺ substituted nanocrystalline Ni-Zn ferrites, J Alloys Compd. 735 (2018) 2532–2543. <https://doi.org/10.1016/J.JALLCOM.2017.11.258>.
- [3]. M.A. Gabal, Y.M. Al Angari, F.A. Al-Agel, Cr-substituted Ni-Zn ferrites via oxalate decomposition. Structural, electrical and magnetic properties, J Magn Magn Mater. 391 (2015) 108–115. <https://doi.org/10.1016/J.JMMM.2015.04.115>.
- [4]. S. Taneja, D. Chahar, P. Thakur, Influence of bismuth doping on structural, electrical and dielectric properties of Ni-Zn nanoferrites, J Alloys Compd. 859 (2021) 157760. <https://doi.org/10.1016/J.JALLCOM.2020.157760>.
- [5]. S. Supriya, Recent trends and morphology mechanisms of rare-earth based BiFeO₃ nano perovskites with excellent photocatalytic performances, Journal of Rare Earths. 41 (2023) 331–341. <https://doi.org/10.1016/j.jre.2022.08.011>.

[6]. M.D. Hossain, M.N.I. Khan, A. Nahar, M.A. Ali, M.A. Matin, S.M. Hoque, M.A. Hakim, A.T.M.K. Jamil, Tailoring the properties of Ni-Zn-Co ferrites by Gd³⁺ substitution, *J Magn Magn Mater.* 497 (2020) 165978. <https://doi.org/10.1016/J.JMMM.2019.165978>.

[7]. S. Ikram, J. Jacob, M.I. Arshad, K. Mahmood, A. Ali, N. Sabir, N. Amin, S. Hussain, Tailoring the structural, magnetic and dielectric properties of Ni-Zn-CdFe₂O₄ spinel ferrites by the substitution of lanthanum ions, *Ceram Int.* 45 (2019) 3563–3569. <https://doi.org/10.1016/J.CERAMINT.2018.11.015>.

[8]. M. Houshiar, L. Jamilpanah, Effect of Cu dopant on the structural, magnetic and electrical properties of Ni-Zn ferrites, *Mater Res Bull.* 98 (2018) 213–218. <https://doi.org/10.1016/J.MATERRESBULL.2017.10.024>.

[9]. N. Lenin, R. Rajesh Kanna, K. Sakthipandi, A. Senthil Kumar, Structural, electrical and magnetic properties of Ni_{1-x}La_xFe₂-xO₄ nanoferrites, *Mater Chem Phys.* 212 (2018) 385393. <https://doi.org/10.1016/J.MATCHEMPHYS.2018.03.062>

[10]. S. Supriya, Synthesis mechanisms and effects of BaTiO₃ doping on the optical properties of Bi_{0.5}Na_{0.5}TiO₃ lead-free ceramics, *J Solid State Chem.* 308 (2022) 122940.

[11]. D. Venkatesh, B.B.V.S. Vara Prasad, K. V. Ramesh, M.N. V. Ramesh, Magnetic Properties of Cu²⁺ Substituted Ni-Zn Nano-Crystalline Ferrites Synthesized in Citrate-Gel Route, *J Inorg Organomet Polym Mater.* 30 (2020) 2057–2066. <https://doi.org/10.1007/s10904-019-01419-2>.

[12]. M. Houshiar, L. Jamilpanah, Effect of Cu dopant on the structural, magnetic and electrical properties of Ni-Zn ferrites, *Mater Res Bull.* 98 (2018) 213–218. <https://doi.org/10.1016/J.MATERRESBULL.2017.10.024>.

[13]. S. Ikram, J. Jacob, M.I. Arshad, K. Mahmood, A. Ali, N. Sabir, N. Amin, S. Hussain, Tailoring the structural, magnetic and dielectric properties of Ni-Zn-CdFe₂O₄ spinel ferrites by the substitution of lanthanum ions, *Ceram Int.* 45 (2019) 3563–3569. <https://doi.org/10.1016/J.CERAMINT.2018.11.015>.

[14]. J. Azadmanjiri, Structural and electromagnetic properties of Ni-Zn ferrites prepared by sol-gel combustion method, *Mater Chem Phys.* 109 (2008) 109–112. <https://doi.org/10.1016/J.MATCHEMPHYS.2007.11.001>.

[15]. S. Taneja, D. Chahar, P. Thakur, A. Thakur, Influence of bismuth doping on structural, electrical and dielectric properties of Ni-Zn nanoferrites, *J Alloys Compd.* 859 (2021) 157760. <https://doi.org/10.1016/J.JALLCOM.2020.157760>.

[16]. M.K. Anupama, B. Rudraswamy, N. Dhananjaya, Investigation on impedance response and dielectric relaxation of Ni-Zn ferrites prepared by self-combustion technique, *J Alloys Compd.* 706 (2017) 554–561.

[17]. S. Ikram, J. Jacob, M.I. Arshad, K. Mahmood, A. Ali, N. Sabir, N. Amin, S. Hussain, Tailoring the structural, magnetic and dielectric properties of Ni-Zn-CdFe₂O₄ spinel ferrites by the substitution of lanthanum ions, *Ceram Int.* 45 (2019) 3563–3569. <https://doi.org/10.1016/J.CERAMINT.2018.11.015>.

[18]. R.H. Kadam, Kirti Desai, Vishnu S. Shinde, Mohd. Hashim, Sagar E. Shirasath, Influence of Gd³⁺ ion substitution on the MnCrFeO₄ for their nanoparticle shape formation and magnetic properties, *Journal of Alloys and Compounds*, 657 (2016) 487–494. <https://doi.org/10.1016/j.jallcom.2015.10.164>

[19]. I.H. Gul, W. Ahmed, A. Maqsood, Electrical and magnetic characterization of nanocrystalline Ni-Zn ferrite synthesis by co-precipitation route, *J. Magn. Magn Mater.* 320 (2008) 270–275, <https://doi.org/10.1016/j.jmmm.2007.05.032>.

[20]. Jyoti Parashar, et al., Dielectric behaviour of Zn substituted Cu nano-ferrites, *J. Magn. Magn Mater.* 394 (2015) 105–110, <https://doi.org/10.1016/j.jmmm.2015.06.044>.

[21]. M. Shoba, S. Kaleemulla, Structural, optical and dielectric studies of Er substituted zincferrite nano spheres, *J. Phys. Chem. Solid.* 111 (2017) 447–457, <https://doi.org/10.1016/j.jpcs.2017.08.028>.

[22]. Zahoor Ahmad, et al., Structural and complex impedance spectroscopic studies of Mg substituted CoFe₂O₄, *Ceram. Int.* 42 (2016) 18271–18282, <https://doi.org/10.1016/j.ceramint.2016.08.154>.

[23]. Xiaolei Qu, et al., Applications of nanotechnology in water and wastewater treatment, *Water Res.* 47 (2013) 3931–3946,

[24]. D. Ravi Kumar, et al., Structural, optical, room-temperature and low temperature magnetic properties of Mg-Zn nanoferrite ceramics, *J. Asian Ceram. Soc.* (2019),

[25]. Dinesh Varshney, Kavita Verma, Substitutional effect on structural and dielectric properties of Ni_{1-x}A_xFe₂O₄ (A=Mg, Zn) mixed spinel ferrites, *Mater. Chem. Phys.* 140 (2013) 412–418.

[26]. Abdalrawf I. Ahmed, et al., Structural and optical properties of Mg_{1-x}Zn_xFe₂O₄ nano-ferrites synthesized using co-precipitation method, *Adv. Nanoparticles* 4 (2015) 45–52.

[27]. S. Asiri, et al., Hydrothermal synthesis of Co_yZn_yMn_{1-2y}Fe₂O₄ nano ferrites: magneto optical investigation, *Ceram. Int.* 44 (2018) 5751–5759.

[28]. Rohit Sharma, et al., Ferrimagnetic Ni²⁺ doped Mg-Zn spinel ferritenanoparticles for high density information storage, *J. Alloys Compd.* 704 (2017) 7–17.

[29]. Amba Mondal et al/Investigation on spectroscopic properties and temperature dependent photoluminescence of NIR emitting Cr³⁺ doped zinc gallate longpersistent nano phosphor, *Phys. B Condens. Matter* 569 (2019) 20–30.

[30]. G.S. Yashavanth Kumar, et al., Synthesis, optical and electrical properties of ZnFe₂O₄, *Nanomater. Nanotechnol.* 2 (1–6) (2012) 19.

[31]. K. Kombaiah, et al., Catalytic studies of NiFe₂O₄ nanoparticles prepared by conventional and microwave combustion method, *Mater. Chem. Phys.* 221 (2019) 11–28, <https://doi.org/10.1016/j.matchemphys.2018.09.012>.

[32]. Erik Casbeer, et al., Synthesis and photocatalytic activity of ferrites under visible light: a review, *Separ. Purif. Technol.* 87 (2012) 1–14.

[33]. Dafeng Zhang, et al., One-step combustion synthesis of CoFe₂O₄–graphene hybrid materials for photodegradation of methylene blue, *Mater. Lett.* 113 (2013) 179–181.

[34]. Caroline Ponraj, et al., Photocatalytic degradation of acid red-85 dye by nickel substituted bismuth ferrite nanoparticles, *Mater. Res. Express* 6 (2019), 084006, 1-11.

[35]. Behnaz Lahijani, et al., Magnetic PbFe₁₂O₁₉-TiO₂ nanocomposites and their photocatalytic performance in the removal of toxic pollutants, *Main Group Met. Chem.* 41 (3–4) (2018) 53–62.

[36]. M.N. Zulfiqar Ahmed, et al., Photocatalytic activity of nanocrystalline ZnO, a-Fe2O3 and ZnFe2O4/ZnO, *Appl. Nanosci.* 5 (2015) 961–968.

[37]. S.K. Jesudoss, et al., Studies on the efficient dual performance of Mn_{1-x}Ni_xFe₂O₄ spinel nanoparticles in photodegradation and antibacterial activity, *J. Photochem. Photobiol. B Biol.* 165 (2016) 121–132, <https://doi.org/10.1016/j.jphotobiol.2016.10.004>.

[38]. M. Madhukara Naik, et al., Green synthesis of zinc doped cobalt ferrite nanoparticles: structural, optical, photocatalytic and antibacterial studies, *Nano-Struct. Nano-Object.* 19 (2019) 100322, <https://doi.org/10.1016/j.nanoso.2019.100322>.

[39]. Pooja Dhiman, et al., Solar active nano-Zn_{1-x}Mg_xFe₂O₄ as a magneticallyseparable sustainable photocatalyst for degradation of sulfadiazine antibiotic, *J. Mol. Liq.* 294 (2019) 111574,

[40]. S.J. Abhishek Nigam, Pawar Structural, magnetic, and antimicrobial properties of zinc doped magnesium ferrite for drug delivery applications, *Ceram. Int.* 46 (2020) 4058–4064, <https://doi.org/10.1016/j.ceramint.2019.10.243>.

[41]. M.I.A. Abdel Maksoud, Gharieb S. El-Sayyad, A. Abokhadra, L.I. Soliman, H.H. El-Bahnasawy, A.H. Ashour, Influence of Mg²⁺ substitution on structural, optical, magnetic, and antimicrobial properties of Mn–Zn ferrite nanoparticles, *J. Mater. Sci. Mater. Electron.* 31 (2020) 2598–2616, <https://doi.org/10.1007/s10854-019-02799-4>.

[42]. M. Madhukara Naik, H.S. Bhojya Naik, G. Nagaraju, M. Vinuth, K. Vinu, R. Viswanath, Green synthesis of zinc doped cobalt ferrite nanoparticles: structural, optical, photocatalytic and antibacterial studies, *Nano-Struct. Nano-Object.* 19 (2019) 100322, <https://doi.org/10.1016/j.nanoso.2019.100322>.

[43]. S.K. Jesudoss, J. Judith Vijaya, L. John Kennedy, P. Iyyappa Rajan, Hamad A. Al-Lohedan, R. Jothi Ramalingam, K. Kaviyarasu, M. Bououdina, Studies on the efficient dual performance of Mn_{1-x}Ni_xFe₂O₄ spinel nanoparticles in photo degradation and antibacterial activity, *J. Photo chem. Photo biol. B Biol.* 165 (2016) 121–132, <https://doi.org/10.1016/j.jphotobiol.2016.10.004>.

